

Influences of upstream extensions on flow around a curved cylinder

Fengjian Jiang^{1*}, Bjørnar Pettersen¹, Helge I. Andersson²

¹Department of Marine Technology, Norwegian University of Science and Technology, NO-7491 Trondheim, Norway

²Department of Energy and Process Engineering, Norwegian University of Science and Technology, NO-7491 Trondheim, Norway

*Corresponding author email: fengjian.jiang@ntnu.no

ABSTRACT: In simulations of flow around a concave curved cylinder, *i.e.* free-stream aligned with the plane of curvature and directed towards the inner face of the curvature, one can not avoid interactions between the cylinder and the inlet boundary. To get rid of the effects brought about by this interaction, we consider different lengths of upstream straight extensions at the lower end of the curved cylinder ($0D$, $5D$ and $10D$, where D is the cylinder diameter), referred to as horizontal extensions. In this study, we directly solve the time-dependent three-dimensional Navier-Stokes equations. Results reveal that the appended horizontal extension allows the boundary layer to develop, so that the velocity profile at the curved cylinder inception is significantly different from the case where no horizontal extension is considered. The laminar boundary layer is thinner than that in the flat plate flow, which is given by Blasius' solution. The results from $5D$ and $10D$ extensions show a clear convergent tendency. We therefore suggest that a horizontal extension is essential for concave curved cylinder flow simulation, and $10D$ would be a preferred choice.

Keywords: curved cylinder; boundary conditions; wakes; boundary layer

NOMENCLATURE

C_{Fi}	Force coefficients $C_{Fi} = F_i / \frac{1}{2} \rho U_0^2 S_p$	t	Time
D	Cylinder diameter	$\mathbf{u} = (u, v, w)$	Instantaneous velocity vector
f	Frequency	$\nabla \mathbf{u}$	Velocity gradient tensor
F_i	Body forces $F_i = (F_x, F_y, F_z)$	$\langle u \rangle, \langle v \rangle, \langle w \rangle$	Time-averaged velocity
p	Pressure	U_0	Inlet (freestream) velocity
Re	Reynolds number $Re = DU_0/\nu$	x, y, z	Coordinates
s	Arc of cylinder centerline	$\delta_{0,99}$	Boundary layer thickness
S	Symmetric part of $\nabla \mathbf{u}$	ν	Kinematic fluid viscosity
S_p	Projection area of geometry	Ω	Antisymmetric part of $\nabla \mathbf{u}$
St	Strouhal number ($St = fD/U_0$)	λ_2	2 nd largest eigenvalue of $(S^2 + \Omega^2)$
ρ	Density		

1. Introduction

We encounter a configuration of a curved cylinder in different marine engineering applications: for example, a flexible riser that connects the seabed and floating offshore structures, mooring lines, or pipelines to transport oil and gas. Due to its curved span, the

wake behind a curved cylinder is considerably more complex than the wake of a straight cylinder, and becomes an interesting research topic. However, compared to the extensive studies on the straight cylinder wake, there are far less published results on a curved cylinder wake.

The curved cylinder is modeled as a quarter segment of a ring in most relevant studies; depending on the specific problem, straight extensions may be added to one or both ends of the quarter ring. Earlier studies of curved cylinders mostly focused on flow normal to the plane of curvature, as reviewed in previous publications^{[1][2]}. (Miliou et al.)^[3] first carried out fundamental studies of curved cylinder wakes with the inflow aligned with the plane of curvature. They studied flow past stationary curved cylinders at low Reynolds numbers of 100 and 500, and systematically reported the shedding pattern and wake topology. (de Vecchi et al.)^[2] also studied the wake of curved cylinders at low Reynolds number $Re = 100$ and they considered both stationary cylinders and cylinders with forced cross-flow oscillations. Both studies observed distinctly different wake topologies when the inflow direction is reversed, i.e. bent vortex shedding when the inflow is towards the outer face of the curvature (referred to as *convex* configuration), but suppressed vortex shedding when the inflow is towards the inner face of the curvature (referred to as *concave* configuration). In addition, both studies attributed the suppression of vortex shedding in the concave configuration to an axial flow along the curvature, which makes the shear layer less susceptible to roll up and subsequently shed as a vortex street. Recently, (Gallardo et al.)^[4] investigated the turbulent wake behind a convex curved cylinder at Reynolds number $Re = 3900$, in which they revealed distinct differences between the wake pattern in the upper part of the curved cylinder wake as compared to that in the lower part. (Xu and Cater)^[5] reported a RANS study of a high Reynolds number flow ($Re = 1.5 \times 10^5$) around a curved cylinder, which was virtually a flexible riser model.

Unlike in simulations of flow past straight cylinders, where periodic boundary conditions are normally used at the two ends of the cylinders, special attention is essential for the boundary conditions at the two ends of the quarter ring. The abovementioned studies^{[1]-[4]} all considered a straight extension normal to the free-stream direction (often referred to as a *vertical* extension) at one end of the quarter ring where a free-slip boundary condition was suggested. (Gallardo et al.)^[6] carefully studied the free-slip boundary condition at this end of the quarter ring and the choice of a reasonable extension length.

It is noteworthy that in the convex configuration, most previous studies^{[2]-[4]} also considered another straight extension aligned with the free-stream direction at the other end of the quarter ring, which is often referred to as a *horizontal* extension. This horizontal extension continues all the way to the outlet of the flow domain. No free end will therefore appear in the cylinder wake. However, when it comes to the concave configuration, the horizontal extension was omitted in most numerical simulations^{[2][3]}. To the authors' knowledge, the only study that considers a horizontal extension of a concave curved cylinder is an experimental investigation^[1]. In that study the horizontal extension has a free end in the fluid and therefore induces additional disturbances to the incoming flow.

In the concave curved cylinder case reported by (Miliou et al.)^[3], one end of the quarter ring interacts directly with the inlet surface. It is rather obvious that this direct interaction between the curved cylinder and inlet has some effects on the flow field. If one consider the most likely application of a curved cylinder, i.e. a deep-sea riser or a pipeline landing on the seabed, the curved part is most likely connected with straight extensions at both ends (horizontal and vertical). In this context, it is always difficult to isolate the curved part (quarter ring) from its straight extensions. Although (Miliou et al.)^[3] gave a special treatment to the inflow boundary condition (as details in Section 2.1, viz equation (1)), the issue was left without any clarification.

In the present study, we aim to investigate the influence of a horizontal extension on the flow around a concave curved cylinder. Free ends in the computational domain are intentionally avoided to eliminate additional disturbances; so the horizontal extensions will start upstream and affect the inlet boundary conditions. Only one Reynolds number $Re = 100$ will be studied, while different lengths of the horizontal extension will be considered. This particular Re was chosen to enable direct comparisons with the results obtained by (Miliou et al.)^[3]. Comparisons of the boundary layer flow along extensions of various lengths will be presented and the influence of the different extensions on the wake behind the curved part of the cylinder will be considered.

2. Numerical setups

2.1 Flow configuration

In this study, we consider a quarter ring curved circular cylinder, and a concave configuration is adopted, i.e. the free-stream is directed towards the inner face of the ring. The geometry and the computational domain are depicted in figure 1. The radius of curvature is $R = 12.5D$, where R indicates the distance between the center of the ring (point O in figure 1) and the center of the circular cross sections, and D is the diameter of the circular cross-section. The Reynolds number is defined based on the free-stream velocity U_0 and D , i.e. $Re = U_0D/\nu$, where ν is the kinematic fluid viscosity.

As shown in figure 1, the geometry studied here consists of three parts: a curved part (quarter ring), and two straight extensions at the two ends of it. We refer to them as the *vertical* (upper) extension and the *horizontal* (lower) extension, respectively. In order to study the effects caused by these straight extensions, we will consider some different combinations. An overview of the different cylinder configurations studied is given in Table 1.

Table 1. List of all cases in this study

Configuration	Vertical extension	Horizontal extension	Re	Domain size $L_x \times L_y \times L_z$
$v0h0$	None	None	100	$28D \times 21D \times 18D$
$v6h0$	6D	None	100	$28D \times 21D \times 24D$
$v6h5$	6D	5D	100	$33D \times 21D \times 24D$
$v6h10$	6D	10D	100	$38D \times 21D \times 24D$

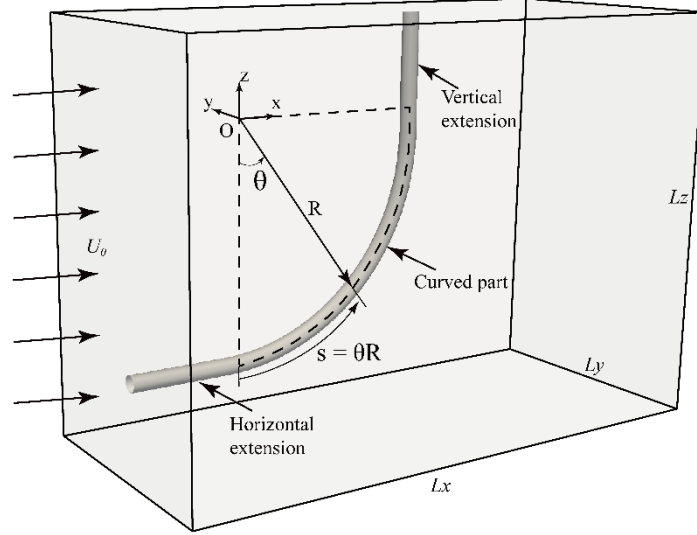


Figure 1. Sketch of the geometry of the concave curved cylinder and the computational domain. The uniform inflow U_0 is from the left.

As depicted in figure 1, we define the streamwise direction as the x -direction, the transverse direction as the y -direction, and the vertical direction as the z -direction, therefore the velocity vector writes $u_i = (u, v, w)$. For all cases, we adopted the same inflow boundary condition as that used by (Miliou et al.)^[3]:

$$\frac{u}{U_0} = 1 - \exp(-50(\sqrt{(\frac{y}{D})^2 + (\frac{z}{D} + 12.5)^2} - 0.5)); \quad \frac{v}{U_0} = \frac{w}{U_0} = 0. \quad (1)$$

This velocity profile mimicks a very thin exponentially growing boundary layer profile at the intersection of the cylinder with the inlet computational boundary. The boundary layer profile defined by equation (1) will be shown later in figure 5. If we follow the most commonly used 0.99-criterion to define the boundary layer thickness $\delta_{0.99}$, equation (1) virtually represents a $\delta_{0.99} = 0.092D$ thick boundary layer, while further away from the cylinder geometry, the incoming free-stream remains uniform as U_0 .

We imposed Neumann boundary conditions for the velocity components ($\partial u/\partial x = \partial v/\partial x = \partial w/\partial x = 0$) and zero pressure ($p = 0$) at the outlet of the flow domain. On the other four sides of the computational domain, we used free-slip boundaries, while the solid surface of the cylinder was treated as a no-slip boundary.

2.2 Numerical method

In this study, we directly solve the full Navier-Stokes equations :

$$\frac{\partial u_i}{\partial x_i} = 0 \quad (2)$$

$$\frac{\partial u_i}{\partial t} + u_j \frac{\partial u_i}{\partial x_j} = -\frac{1}{\rho} \frac{\partial p}{\partial x_i} + \nu \frac{\partial^2 u_i}{\partial x_j \partial x_j} \quad (3)$$

with a second-order finite-volume code MGLET^[7]. Equations (2) and (3) are discretized on a 3-dimensional staggered Cartesian grid. The discretized equations are integrated in time with Williamson's 3rd-order Runge-Kutta scheme^[8], while pressure corrections are

achieved by using Stone’s strongly implicit procedure (SIP)^[9]. The representation of the cylindrical geometry inside the Cartesian grid is accomplished by an immersed boundary method (IBM), which was described in detail by Peller et al. ^[10]. The same code has recently been used for the same curved cylinder, but with an opposite flow direction (so-called convex configuration) ^{[4][11]}.

2.3 Grid sensitivity study

We used only the curved part of the cylinder (i.e. configuration $\nu 0h0$ in Table 1) for a grid sensitivity study. Table 2 gives detailed information of the cases studied. Here we define the body force coefficients as $C_{Fi} = F_i / 0.5\rho U_0^2 S_p$, where S_p is the projected area of the curved cylinder in the streamwise direction. In cases *A*, *B* and *C* in table 2, we kept Δz_{\min} unchanged while using different $\Delta x_{\min} = \Delta y_{\min}$ in order to investigate grid sensitivity in the (x, y) -plane. The data obtained from Cases *A*, *B* and *C* clearly show that $\Delta x_{\min} = \Delta y_{\min} = 0.05D$ is fine enough from a grid-convergence point of view. Cases *C* and *D* in Table 2 aimed to reveal grid sensitivity in the z -direction, but the data indicates that the computational results are insensitive to the grid size in the z -direction. Therefore, the grid sizes of Case *C* are adopted in all further simulations. In addition, Table 2 lists reference results from a previous study^[3]. Note that the wake of the $\nu 0h0$ configuration is symmetric and steady (as shown in figure 2(a) and (b)), therefore C_{Fy} in Table 2 should ideally be zero.

Table 2. Grid study cases for configuration $\nu 0h0$

Case	$(\Delta x = \Delta y)_{\min}/D$	$\Delta z_{\min}/D$	C_{Fx}	C_{Fy}	C_{Fz}
A	0.1	0.08	1.06	0.0012	0.43
B	0.08	0.08	1.00	0.0008	0.41
C	0.05	0.08	0.978	0.0003	0.41
D	0.05	0.05	0.987	0.0002	0.41
(Miliou et al. 2007) ^[3]	-	-	1.0745	0.0001	0.42

3. Validation cases

In order to validate the numerical method and the computational setup used in this study, we conducted two validation cases, i.e. $\nu 0h0$ and $\nu 6h0$, with the aim to compare with the corresponding results in (Miliou et al.)^[3]. Figure 2 shows the vortical structures, which are presented by the iso-surface of $\lambda_2 = -0.01$. λ_2 has been a widely used indicator for vortex cores since it was first proposed by (Jeong & Hussain)^[12]. It is defined as the second largest eigenvalue of $S^2 + \Omega^2$, where S and Ω are the symmetric and antisymmetric parts of the velocity gradient tensor $\nabla \mathbf{u}$.

Figure 2(a) and 2(b) show a comparison of the vortical structure behind the $\nu 0h0$ configuration, from which we clearly observe that the vortical structures obtained from the present study (a) well resembles that from the literature^[3] (b). All three components of the monitored body forces are steady because vortex shedding is suppressed by the axial flow in this particular case. Figure 2(c) and 2(d) also show good agreement between results from the present study and that from Miliou et al. ^[3] for configuration $\nu 6h0$. The main features

of the flow around this cylinder configuration, i.e. suppressed vortex shedding behind the curved part together with conventional vortex shedding behind the vertical extension, were accurately captured.

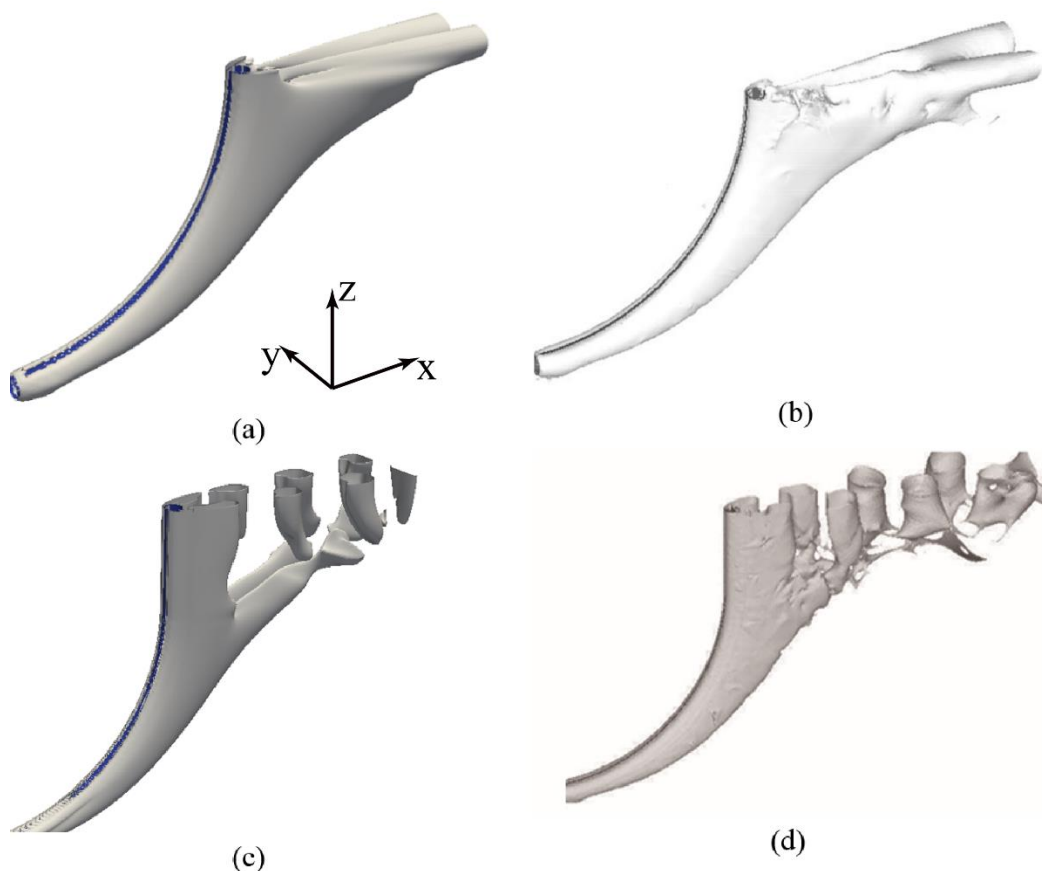


Figure 2. Qualitative comparisons of computed vortical structures and those reported in the literature^[3]. (a) and (b) are $v0h0$ configuration, (c) and (d) are $v6h0$ configuration. (a) and (c) are from current study, while (b) and (d) are from Miliou et al.^[3]. All plots show the iso-surface of $\lambda_2 = -0.01$. Note that the coordinate system in (a) just indicates the directions, but not location of the origin.

Figure 3(a) shows the pressure distribution in the symmetry plane, i.e. the (x,z) -plane at $y/D = 0$ for the $v0h0$ configuration. Figure 3(b)-(e) show the streamwise velocity (u/U_0) contour plots in four different horizontal planes (i.e. (x,y) -planes) whose locations are $z/D = 0, -2, -5,$ and $-8,$ respectively. Figure 3 is meant to be visually compared (qualitatively) with figure 10 in (Miliou et al.)^[3]. Figure 3(b)-(e) show that the flow is symmetric at all four different vertical locations. We also see that the wake becomes narrower as the vertical plane moves from the top of the curved cylinder to the lower part. All these results agree perfectly well with those in [3]. The observed variation of the wake width can be explained by the change of local cross-sectional shape. Due to the curvature of the cylinder, the cross-sectional shape in the (x,y) -plane changes from a perfect circle at the upper top of the curved cylinder to an ellipse in the lower part. In addition, the aspect ratio of the cross-

sectional ellipse increases downward. In this case, the slender cross-section leads to a more steady and narrow wake. The same phenomenon was also observed in the wake of an inclined prolate spheroid ^[13], where the inclination of the geometry similarly led to different cross-sectional shapes.

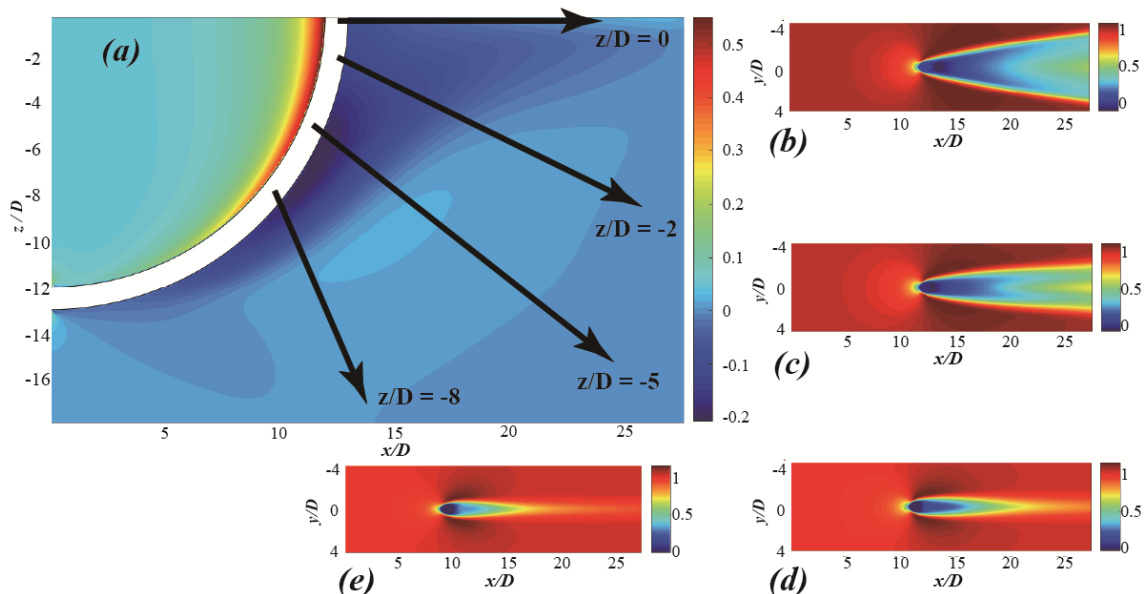


Figure 3. Flow fields for configuration $v0h0$. (a) Pressure distribution in the symmetry plane, *i.e.* the (x,z) -plane at $y/D = 0$; (b)-(e) Streamwise velocity contour plots at four different (x,y) -planes whose locations are $z/D = 0, -2, -5,$ and $-8,$ respectively.

4. Influences of horizontal extensions

In this section, we will discuss how a horizontal extension affects the flow field around the concave curved cylinder by comparing the results for three different configurations: $v6h0$, $v6h5$, and $v6h10$. A quick check of the streamwise body force coefficient (C_{Fx}) on the curved part and the shedding frequency ($St = fD/U_0$) of the three configurations are provided in Table 3, from which we somewhat surprisingly do not see any distinct differences between the three different cylinder configurations.

Table 3. Force coefficient and frequency for different configurations

Configuration	Horizontal extension	C_{Fx} on the curved part	St (frequency)	Reference St^*
$v6h0$	0D	1.066	0.108	0.1123
$v6h5$	5D	1.013	0.106	-
$v6h10$	10D	1.0	0.103	-

* The reference St is from (Miliou *et al.*) ^[3], configuration $v6h0$.

In order to investigate how the flow develops along the horizontal extensions in more detail, we look at the time-averaged streamwise velocity $\langle u \rangle / U_0$ along the horizontal cylinder in the symmetry plane at $y/D = 0$, and at different distances δh away from the

cylinder surface (in positive z -direction). In figure 4, we present data from the $v6h10$ configuration. It is noteworthy that the results from the $v6h5$ configuration coincide perfectly with the first $5D$ of the $v6h10$ configuration. A dashed vertical line is therefore inserted in figure 4 to indicate where the $v6h5$ configuration stops. Five different δh (0.1, 0.2, 0.3, 0.4 and 0.5, respectively) were chosen to also have an impression of how the flow field develops in the normal-to-surface direction. One should recall that for all different configurations considered here, we imposed the same inlet boundary condition (equation (1)). As already mentioned, this boundary condition gives a $\delta_{0.99} = 0.092D$ thick boundary layer; whereas the first $\langle u \rangle / U_0$ line in figure 4 is already $\delta h = 0.1D$ away from the cylinder surface. Therefore all curves in figure 4 begin at $x/D = -10$ with a value of $\langle u \rangle$ very close or equal to the free-stream velocity U_0 .

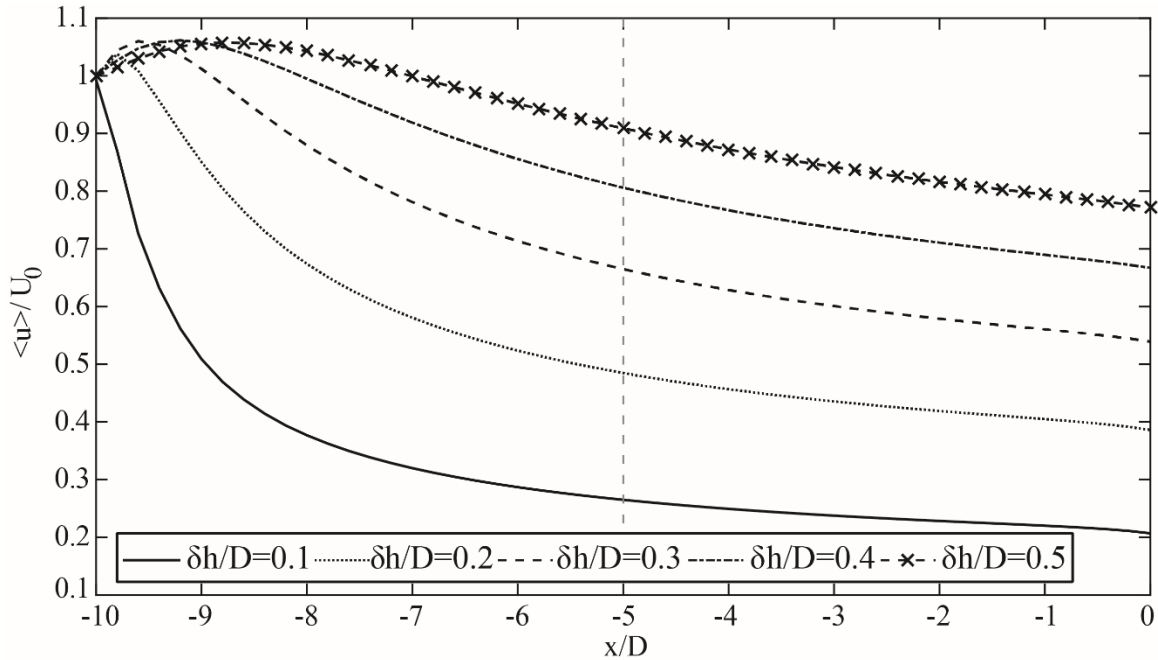


Figure 4. Streamwise velocity $\langle u \rangle / U_0$ distribution along the horizontal extension in the symmetry plane and at different distances $\delta h / D$ away from the cylinder surface. The results are from the $v6h10$ configuration. The vertical dashed line at $x / D = -5$ indicates the location where the $5D$ extension of the $v6h5$ configuration would have stopped.

From figure 4 it is clear that the streamwise velocity $\langle u \rangle$ changes considerably over the first $5D$ of the horizontal extension. The smaller δh is, the greater the changes in $\langle u \rangle$ are. At $\delta h = 0.1D$, we observe that after a distance of $5D$ from the inlet, the streamwise velocity dropped to less than 30% of the free-stream velocity. Even if we look at the farthest location from the cylinder, i.e. when $\delta h = 0.5D$, $\langle u \rangle / U_0$ has changed to about $0.9U_0$ after a distance of $10D$. Whereas after a distance of $5D$ along the horizontal extension, $\langle u \rangle / U_0$ changes relatively less. But it is still interesting to notice the different $\langle u \rangle / U_0$ values at position $x/D = -5$ and $x/D = 0$ in figure 4, because they indicate how different the flows in the $v6h5$ and $v6h10$ configurations are when they reach the curved part of the cylinder, i.e.

at position $x/D = 0$ in figure 4. Figure 5 offers a more straightforward comparison of the boundary layer profile exactly at position $x/D = 0$, i.e. at the interface between of the horizontal extension and the curved part. We can see that the boundary layers in both $v6h5$ and $v6h10$ configurations are thicker than $\delta_{0.99} = 0.092D$ given by the inlet boundary condition in equation (1).

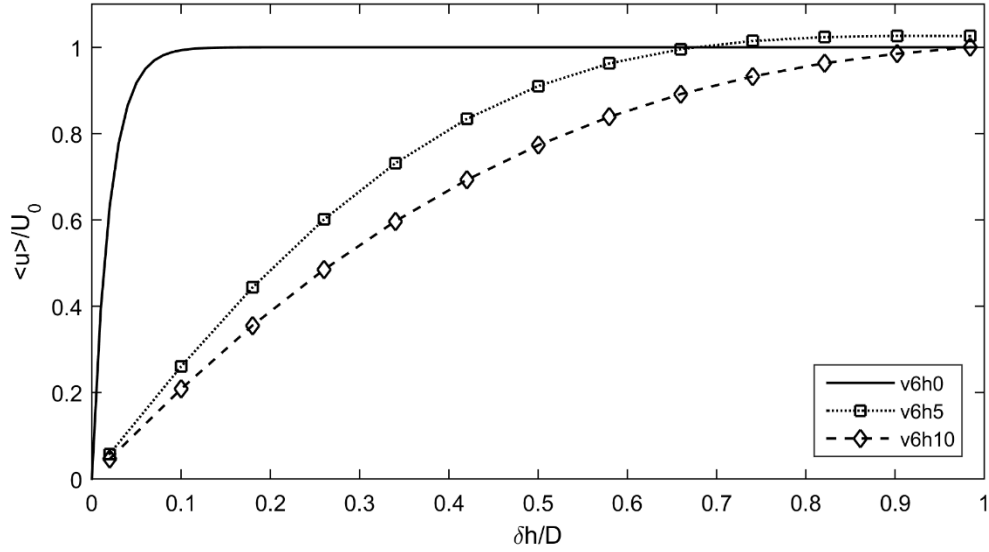


Figure 5. Boundary layer velocity profiles at position $x/D = 0$ in the symmetry plane for all configurations. The profile for the $v6h0$ configuration is that defined by equation (1), whereas the two other profiles demonstrate how the boundary layer develops along the horizontal extension before it meets the curved part of the cylinder at $x/D=0$.

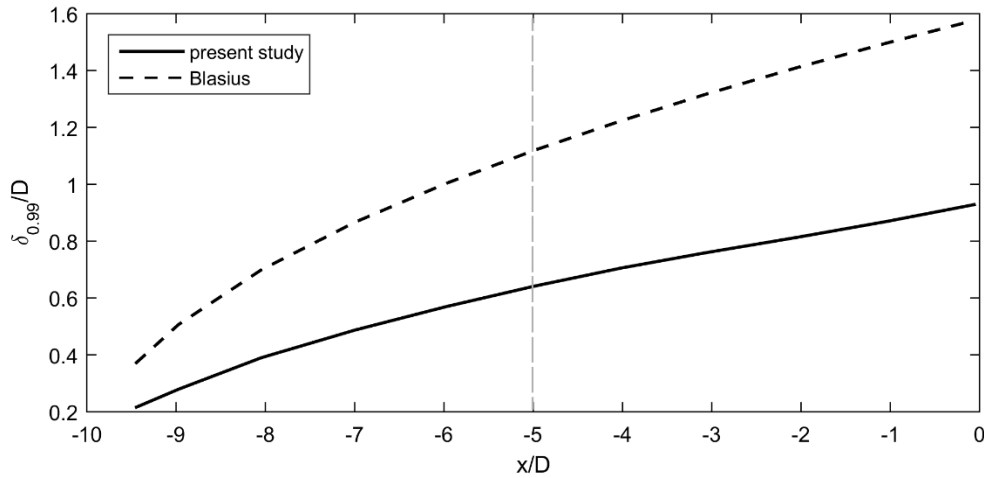


Figure 6. Boundary layer thickness $\delta_{0.99}$ along the horizontal extension in the symmetry plane for configuration $v6h10$. The vertical dashed line at $x/D = 5$ indicates the location where a $v6h5$ configuration would have stopped.

Figure 6 shows the boundary layer thickness $\delta_{0.99}$ along the horizontal extension obtained from the present simulation of the $v6h10$ configuration. Similarly as in figure 4,

results for the first $5D$ length coincide perfectly with the corresponding results for the $v6h5$ configuration. $\delta_{0.99}$ in figure 6 is calculated based on data only in the symmetry plane, i.e. no circumferential average was taken. The boundary layer thickness from the Blasius solution for a laminar flat plate boundary layer, defined by equation (4) (White, 2005, p. 232)^[14], has also been provided for comparisons:

$$\delta_{0.99} = 5.0(vx/U_0)^{1/2} \quad (4)$$

where v here denotes the kinematic fluid viscosity. The boundary layer development along long thin cylinders in axial flow has been studied for decades, see for example the reviews by (Willmarth et al.)^[15] and more recently by (Tutty)^[16]. Although most of the research focused on higher Reynolds numbers (generally over $Re = 1000$), it is generally accepted that the boundary layer thickness for flow along a long thin cylinder is clearly smaller compared to that for a flat plate^[16]. This is in accordance with the result shown in figure 6.

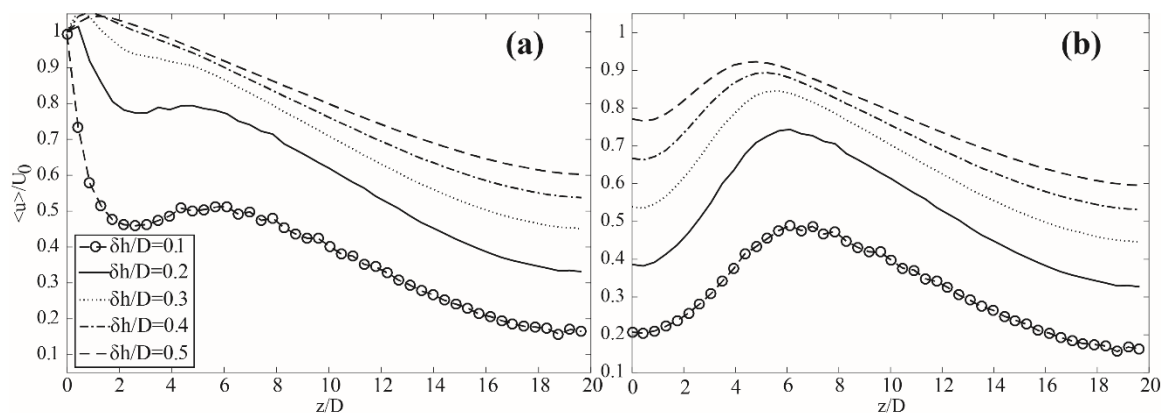


Figure 7. $\langle u \rangle / U_0$ along the concentric quarter-rings $\delta h / D = 0.1, 0.2, 0.3, 0.4, 0.5$ away from the surface (in upstream direction) of the curved cylinder in the symmetry plane. (a) $v6h0$ configuration; (b) $v6h10$ configuration.

The effects brought about by the horizontal extension naturally extends to the curved part. Similarly as in figure 4, we picked out $\langle u \rangle / U_0$ results along the curvature of the curved cylinder in the symmetry plane at different normal distances δh away from the surface (in upstream direction). These are virtually a set of concentric quarter-rings with different radius. We use the arc of the curved cylinder centerline to indicate the location along the curved cylinder, i.e. s/D (as shown in figure 1.). Figure 7 shows $\langle u \rangle / U_0$ along these concentric quarter-rings for both the $v6h0$ and $v6h10$ configurations, from which we observe the different velocity distributions for both configurations. Over the first $s = 2D - 3D$ ($\theta \approx 9^\circ - 13^\circ$) in figure 7(a), we notice that $\langle u \rangle / U_0$ experiences a similar development as shown in the first $5D$ length of figure 4; while this scenario is distinctly different in figure 7(b). In the $v6h10$ configuration, the flow has already developed along the $10D$ long horizontal extension, therefore in the beginning of figure 7(b), $\langle u \rangle$ starts with relatively low values and experiences a smooth increment until it reaches a peak at about $s = 5D - 7D$ ($\theta \approx 23^\circ - 32^\circ$) dependent on δh . The lower two curves in figure 7(a) also show that $\langle u \rangle$ experiences the same increment as in figure 7(b). However, this becomes less clear for δh

larger than $0.3D$. It is worth mentioning that (Miliou et al.)^[3] did not report any peak of streamwise velocity, obviously because they did not have any horizontal extension upstream of the curved cylinder.

Figure 8 shows data only at $\delta h/D = 0.3$, but from all three configurations, put together for the sake of comparison. In figure 8, we also include data from (Miliou et al.)^[3] which is the same case as the $v6h0$ configuration in the present study. From figure 8 we observe that the horizontal extension has a major influence on the streamwise velocity distribution along the quarter ring. In figure 8(b) the vertical velocity distributions $\langle w \rangle$ for different configurations are different from each other but all exhibit roughly the same tendency. The vertical velocity peak is predicted for all three configurations at almost the same location, i.e. at $\theta \approx 46^\circ$ ($s/D \approx 10$). This is also in good agreement with (Miliou et al.)^[3]. However in figure 8(a) we observe that both the $v6h0$ configuration in the present study and in (Miliou et al.)^[3] fail to predict the streamwise velocity peak, whereas the $v6h5$ and $v6h10$ configurations capture this peak, although at slightly different locations.

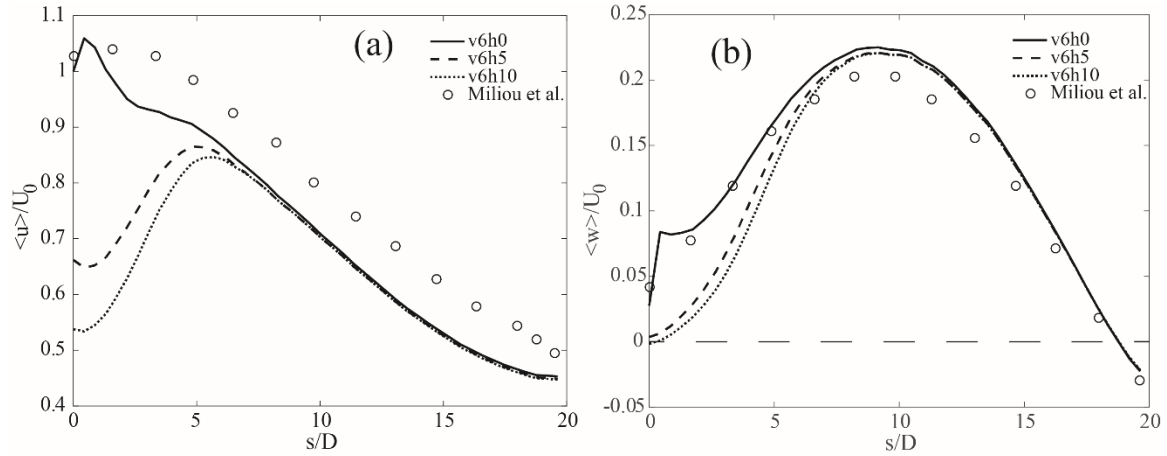


Figure 8. (a) $\langle u \rangle / U_0$ along the curved cylinder at $\delta h/D = 0.3$ away from the cylinder surface for the three different configurations; (b) same as (a) but for $\langle w \rangle / U_0$.

When we study flow around curved cylinders, the axial flow along the curvature is always important, as revealed in several previous studies^{[2][3]}. The axial flow combines information from both the streamwise and vertical velocity components and offers a straightforward description of the flow. Figure 9 displays the axial velocity distribution along the curved part all the way to the end of the vertical extension in the symmetry plane, and at $\delta h/D = 0.3$ upstream of the cylinder surface for all three configurations. The axial velocity vel_{axial} is calculated based on the local $\langle u \rangle$, $\langle w \rangle$ and the angle θ , while for the vertical extension part, the axial velocity becomes equal to $\langle w \rangle$. In figure 9, although both $\langle u \rangle$ and $\langle w \rangle$ are considered, we still observe distinct differences between the $v6h0$ configuration and the other two along the initial curved part (before $s/D \approx 5$, equivalently $\theta \approx 23^\circ$). A comparison between the $v6h5$ and $v6h10$ configurations shows that the resulting axial velocities are somewhat different in values but the tendencies are all the same. It is particularly important to notice that an axial velocity peak at $s/D \approx 5$ is predicted for all

three configurations. Moreover, although the results for the different configurations are rather different in the early part of the flow, they coincide with each other after $s/D \approx 10$, or equivalently $\theta \approx 46^\circ$.

From figure 9, we observe a positive axial flow almost along the whole span, and the axial velocity is rather large along the lower part of the curved cylinder. However, after the velocity peak at $s/D \approx 5$, the axial velocity drops dramatically. It is interesting to notice that as the flow approaches the vertical extension, the axial velocity attains small negative values and remains negative all the way to the end of the $6D$ vertical extension (i.e. to the upper boundary of the computational domain). Such negative values can also be observed in figure 8(b) and are in good agreement with the results reported in [3].

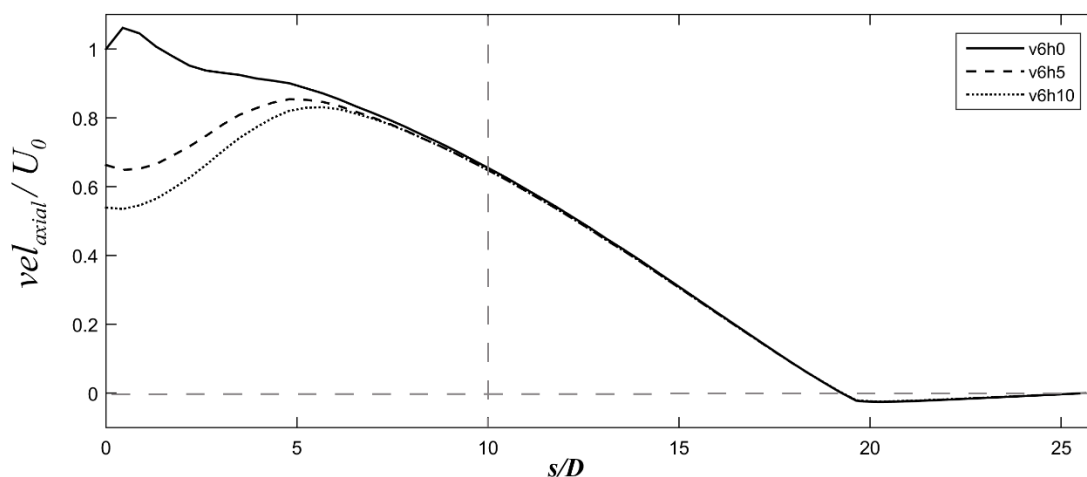


Figure 9. The axial velocity along the curved cylinder (including the $6D$ vertical extension), taken at $\delta h/D = 0.3$ away from the cylinder surface.

5. Concluding remarks

In this paper, we have presented results from a series of simulations of the flow around some different concave curved cylinder configurations. The simulations were conducted by directly solving the full Navier-Stokes equations in space and time. The discussions focus primarily on the influences brought about by the horizontal extension, for which three different lengths: $0D$ ($v6h0$), $5D$ ($v6h5$), and $10D$ ($v6h10$), are considered.

We adopt an analytical inlet boundary condition from a previous study [3], where no horizontal extension was considered. The given inlet boundary condition (equation (1)) is virtually a thin exponential boundary layer velocity profile. In the cases where horizontal extensions were included, we notice that the streamwise velocity experiences abrupt changes over the first $2-3D$, as shown in figure 4. The streamwise velocity drops considerably along the $5D$ or $10D$ long horizontal extensions before the flow reaches the curved part (a quarter ring). Therefore, the velocity profiles at the lower end of the curved cylinder is very different depending on whether a horizontal extension is considered or not.

The comparison of boundary layer profiles at the inception of the curved part reveals that the given inflow profile (equation (1)) provides a too thin boundary layer to be imposed

directly at the lower part of the curved cylinder. We also tracked the development of the boundary layer thickness along the horizontal extension and observed that the boundary layer thickness generally becomes thinner than that given by the Blasius solution for flat plates. This is in good agreement with previous studies (Tutty) ^[16], where a wide range of Reynolds numbers were studied from the laminar to the turbulent flow regime.

By including the horizontal extension, we could capture local peak values for both streamwise velocity and vertical velocity at different axial locations along the curved cylinder. However, for the configuration ($v6h0$) without a horizontal extension, only a peak for the vertical velocity was found, in line with the earlier simulation reported by Miliou et al. ^[3].

The results and discussions in this paper reveal that the horizontal extension has surprisingly strong influences on the flow around a concave curved cylinder. Although this computational study has been performed at one low Reynolds number $Re = 100$, we believe that the qualitative findings are valid also for flows at somewhat higher Reynolds numbers as long as the boundary layer that develops along the horizontal extension remains laminar. In this study, we have shown that the flow takes at least a distance of $5D$ to develop itself properly. This means that at least a $5D$ long horizontal extension will be needed in order to get reasonable results for the concave curved cylinder flow. By comparing results obtained for the $5D$ and $10D$ horizontal extension configurations, we are inclined to conclude that a $10D$ extension would be the preferred choice.

Acknowledgements

This study was supported by the Future Industry's Leading Technology Development program (No. 10042430) of MOTIE/KEIT of Korea. The work has also received support from the Research Council of Norway (Program for Supercomputing) through a grant of computing time.

References

- [1] Assi G.R.S., Srinil N., Freire C.M., Korkischko I. 2014. Experimental investigation of the flow-induced vibration of a curved cylinder in convex and concave configurations. *J. Fluids Struct.* **44**, 52-66
- [2] de Vecchi A., Sherwin S.J., Graham J.M.R. 2008. Wake dynamics of external flow past a curved circular cylinder with the free-stream aligned to the plane of curvature. *J. Fluids Struct.* **24**, 1262-1270
- [3] Miliou A., de Vecchi A., Sherwin S. J., Graham J.M.R. 2007. Wake dynamics of external flow past a curved circular cylinder with the free stream aligned with the plane of curvature. *J. Fluid Mech.* **592**, 89-115
- [4] Gallardo J.P., Andersson H.I., Pettersen B. 2014. Turbulent wake behind a curved circular cylinder. *J. Fluid Mech.* **742**, 192-229
- [5] Xu T., Cater J.E. 2017. Numerical simulation of flow past a curved cylinder in uniform and logarithmic flow. *Ships Offshore Struct.* **12**, 323-329
- [6] Gallardo J.P., Andersson H.I., Pettersen B. 2013. Effects of free-slip boundary conditions on the flow around a curved circular cylinder. *Comput. Fluids.* **86**, 389-394
- [7] Manhart M., Tremblay F., Friedrich R. 2001. MGLET: a parallel code for efficient DNS and LES of complex geometries. In: *Parallel Computational Fluid Dynamics – Trends and Applications*. Elsevier, Amsterdam, pp. 449-456
- [8] Williamson J.H. 1980. Low-storage Runge-Kutta schemes. *J. Comput. Phys.* **56**, 48-56

- [9] Stone H.L. 1968. Iterative solution of implicit approximations of multidimensional partial differential equations. *SIAM J. Numer. Anal.* **5**, 530-558
- [10] Peller N., Le Duc A., Tremblay F., Manhart M. 2006. High-order stable interpolations for immersed boundary methods. *Int. J. Numer. Meth. Fluids* **52**, 1175-1193
- [11] Gallardo J.P., Pettersen B., Andersson H.I. 2014. Coherence and Reynolds stresses in the turbulent wake behind a curved circular cylinder. *J. Turbul.* **15**, 883-904
- [12] Jeong J., Hussain F. 1995. On the identification of a vortex. *J. Fluid Mech.* **285**, 69-94
- [13] Jiang F., Gallardo J.P., Andersson H.I. 2014. The laminar wake behind a 6:1 prolate spheroid at 45° incidence angle. *Phys. Fluids* **26**, 113602
- [14] White F.M. 2005. Viscous Fluid Flow (Third Edition). *McGraw-Hill*. P.232
- [15] Willmarth W.W., Winkel R.E., Sharma L.K., Bogar T.J. 1976. Axially symmetric turbulent boundary layers on cylinders: mean velocity profiles and wall pressure fluctuations. *J. Fluid Mech.* **76**, 35-64
- [16] Tutty O. R. 2008. Flow along a long thin cylinder. *J. Fluid Mech.* **602**, 1-37